Transactions of the **14th International Conference on Structural Mechanics in Reactor Technology** (SMiRT 14), Lyon, France, August 17-22, 1997

GW/11

Ductile tearing predictions in a 304L stainless steel

Marques Vieira E.[(1)], **Louvigné P.F.**[(2)], **Gilles Ph.**[(1)]
(1) Framatome, France
(2) DGA, France

ABSTRACT :

Nowadays, the existence of geometry effects on fracture characteristics measurements is well established whatever the fracture mechanisms are, cleavage or ductile fracture. So far, this was established for materials which have initiation J_{Ic} values less or equal to a few hundreds of kJ/m^2. The present study investigates an extreme material behaviour with high ductility, important deformation and very high fracture toughness. In a first stage, results on geometry effects are presented. Then local criteria are applied to predict these effects.

1. INTRODUCTION.

Geometry effects on cracked specimen are clearly observed for numerous materials for which the single parameter approach is not sufficient to characterise the near fully yielded crack tip states. To overcome this difficulty, several approaches on fracture mechanics have been developed and widely discussed during the last 15 years. On the one hand, fracture is predicted from purely mechanical point of view on the analysis, is treated in terms of two parameter criteria : K-T and J-Q for example. Only the J-Q methodology of O'Dowd and Shih[1] is presented here, where Q is a non-dimensional 'stress' quantifying the level of hydrostatic stress ahead of the crack tip. The combination of the two parameters (J_{Ic}-Q) at fracture initiation defines the fracture toughness locus. On the other hand, local approaches give to fracture analysis an alternative description of the material, in which microstructure damage mechanisms are taken into account. A critical damage parameter Dc is calculated from a conventional relationship such as :

$$Dc = \int_{\varepsilon_0}^{\varepsilon_c} f\left(\frac{\sigma_m}{\sigma_{eq}}, \varepsilon_{eq}^{pl}\right) d\varepsilon_{eq}^{pl} \qquad (1)$$

where σ_m/σ_{eq} is the triaxiality rate and ε_{eq}^{pl} the equivalent plastic strain. Axisymmetric notched tensile specimens AER and cracked specimens are employed to determine the overall fracture strain ε_c, the critical damage Dc and a critical size λ_c.

The present paper describes metallurgical and mechanical properties of 304L stainless steel. After the determination of the fracture toughness locus with the J-Q approach, a local approach is applied to predict geometry effects and the fracture toughness locus.

2. MATERIAL.

2.1. *Chemical composition and tensile properties.*

Micrographic analysis of 304L stainless steel reveals that the matrix is mainly austenitic with some percent of ferrite. Only two types of inclusions have been identified by a chemical analysis(EMPA) : oxides and some alumina particles of typically 4µm diameter. A fully quantitative metallography analysis gives a precise description of the grain size (80µm) and inclusions in 304L steel in terms of : volume fraction (0.065%), average distance between inclusions (≈150µm whatever the direction). **Table 1** summarises the mechanical properties of the 304L at 300°C in longitudinal direction. The work-hardening exponent n is determined by fitting over a large range of deformation the experimental behaviour with the elastic plastic power law $\sigma = K\varepsilon^n$.

Chemical composition	**C**	**Cr**	**Ni**	**Mo**	**Al**	**O**
	0.023	19.0	9.6	0.45	0.014	0.0061
Tensile properties	**E (GPa)**	**YS (MPa)**	**UTS (MPa)**	**elongation (%)**	**Reduction in area (%)**	**n**
	170	158	434	46	60	0.3

Table 1 : Chemical composition in weight percent and tensile properties at 300°C.

2.2. *Determination of the mean strain at fracture.*

To determine the ductility at fracture on 304L stainless steel, tests on axisymmetric notched specimens (AER) are performed at 300°C. Several stress states are obtained by varying the notched radius. The usual relation $\varepsilon_R = 2\ln(\phi_0/\phi_r)$, where ϕ_0 is the initial diameter of the minimum section and ϕ_r is the diameter at failure, is applied. The mean strain at failure is reported in **Table 2** for the three geometries.

	AER2	**AER4**	**AER10**
$\varepsilon_R = 2\ln(\phi_0/\phi_r)$ **(%)**	79.5	85.5	102.4
scatter (%)	8.6	10	4.9

Table 2 : Ductility of notched specimen.

3. CALCULATION OF FRACTURE TOUGHNESS LOCUS.

3.1. *The J-Q approach.*

In J-Q approach, introduced by O'Dowd and Shih[1], the near tip stress and strain states are characterised by the second parameter Q in a range of specimen geometries. Q defines the difference between the stress calculated in a studied specimen and the stress in a reference stress field at a distance $2J/\sigma_{YS}$ from the crack tip :

$$\sigma_{ij} = \sigma_{ij}^{REF} + Q\sigma_{YS}\delta_{ij} \qquad (2)$$

Due to the high deformation in 304L stainless steel, the HRR field has been chosen for the reference stress field. Then, the parameter Q is calculated by :

$$Q = \frac{\sigma_\theta - \sigma_\theta^{HRR}}{\sigma_{YS}} \quad \text{for } r = 2J/\sigma_{YS} \text{ and } \theta = 0. \qquad (3)$$

O'Dowd and Shih[1] have determined Q on several geometries and for different deformation under mechanical monotonous loading. For all cases examined, the range of Q values was about -2 to 2.

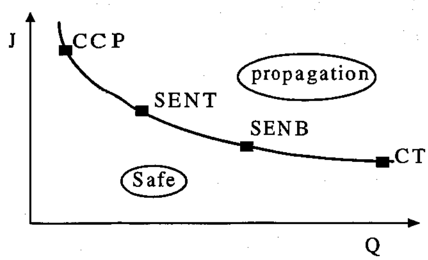

Figure 1 : Fracture toughness locus diagram.

An important number of fracture specimens with several geometries and initial crack lengths has been tested to build up the fracture toughness locus. It is a monotonous curve determined by all J_{Ic}-Q couples (see **Figure 1**). For a given material, O'Dowd and Shih[1] propose that the J_{Ic}-Q fracture toughness locus is unique.

As long as the applied J-Q curve for a given specimen does not intersect the fracture toughness locus, there is no propagation. But, when there is intersection the crack propagation is expected.

3.2. *Application of J-Q approach for 304L stainless steel.*

3.2.1. Geometry of cracked specimens.

To study the geometry effects on fracture toughness, several cracked specimens are tested at 300°C. Two bending geometries are used : conventional Cracked Tension specimens (CT35) with a/W=0.59 and a thickness of 35mm, and Single Edge Notched specimens in Bending (SENB22) with a/W=0.42 and a thickness of 22mm. Single Edge Notched specimens in tension (SENT22) are tested with a/W=0.42 and a thickness of 22mm. These specimens were tested under clamped conditions which strongly limitate the rotation. All the specimens were 20% side-grooved.

3.2.2. Calculation of J.

The ASTM E813-89 procedure gives a specific method to compute J for CT specimens with deep cracks (a/W>0.55). The J integral was estimated by the following formulation :

$$J = \frac{\eta_\delta \ U}{B_N (W - a_0)} \tag{4}$$

where U is the area under the curve giving the load (P) versus the crack mouth opening displacement (δ), B_N is the specimen net thickness and a_0 is the initial crack length.

The η_δ coefficient is evaluated using a finite element method (ABAQUS) for the SENT specimens and work-hardening exponent n ranges from 0.2 to 0.4 :

$$\eta_\delta^{SENT} = 1.03 - 0.277(a_0/W) - 0.7(a_0/W)^2 \qquad \text{for } 0.35 \le a_0/W \le 0.6 \tag{5}$$

For SENB specimens, we have selected Bauvineau[2]'s formulation, base on Dawes[3]'s method, where J is separated in elastic and plastic components :

$$J = J_e + J_{pl} \tag{6}$$

Bauvineau[2] used a standard formulation for the elastic component :

$$J_e = \frac{K^2(1 - \nu^2)}{E} \tag{7}$$

and a formulation similar to the ASTM procedure :

$$J_{pl} = \frac{\eta_{\delta pl} \, U_{pl}}{B_N (W - a_0)} \quad (8)$$

where U_{pl} is the area under the load (P) versus plastic component of load line displacement curve. Bauvineau[2] obtained the following results for n equal 0.27 :

$$\eta_{\delta pl}^{SENB} = 3.695 - 1.772(a_0/W) \qquad \text{for } 0.05 \le a_0/W \le 0.77 \quad (9)$$

3.2.3. Calculation of CTOD.

The crack extension, Δa, is measured by direct observations on the crack surface of the specimen. It includes the blunting size and the physical extension of the crack (see **Figure 2**).

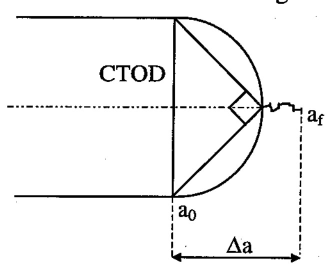

Figure 2 : Crack-tip opening displacement diagram.

For a stationary crack, the crack tip opening displacement (CTOD) is given by the points where 45° lines drawn from crack tip intercept the crack faces (as show in **Figure 2**). The blunting size is equal to CTOD/2 until the crack propagates. The relation between CTOD and J is given by McMeeking[4] :

$J = M \, \sigma_{YS} \, CTOD$

where for a variety of materials the constant M is found to be in a range from 2 to 4 for a CT specimen.

The calculation of CTOD is performed by a finite element method. For each value of J, the size of CTOD is determined by the gap between opposite faces of the deformed crack tip. The results are :

$M = 4.487$ for CT specimen with a/W=0.59 (11)

$M = 4.323$ for SENB specimen with a/W=0.41 (12)

$M = 3.885$ for SENT specimen with a/W=0.41. (13)

The M values difference for the three geometries is not very large. We find similar results between the different specimens.

3.2.4. J_a determination on cracked specimens.

The J-R curves on cracked specimens are obtained with multiple specimen technique. For all cracked specimens, the thickness is lower than $25J_{Ic}/\sigma_Y$. Consequently, our tests do not ensure the validation of J_{Ic} in ASTM E813-89 procedure. Experimental results are presented in **Figure 3**, where blunting lines for the three specimens are determined by:

$J = M \, \sigma_{YS} \, CTOD/2$ (14)

where M is given by (11), (12)&(13). In the ASTM procedure, the blunting line is calculated from material flow properties :

$J = 4 \, \sigma_Y \, CTOD/2$ (15)

	J_{Ic} ASTM	J_a (Figure 3)	dJ/da
CT specimen	1771	1423	652
SENB specimen	2041	1615	786
SENT specimen	1428	1381	583

Table 3 : Cracked specimens results.

The intersection of the regression line determined from specimens results with the blunting line shifted of 0.2mm, defines a value denoted J_a and J_{Ic} refers to results obtained by the

ASTM procedure. We present in **Table 3** both methods results and in **Figure 3** the results that stem from the first method.
The J_{Ic} values are larger than the J_a values. But generally, the J_{Ic} or J_a values are very high. The original result is that J_{Ic} or J_a values and dJ/da slopes are larger in bending specimens than in tension ones. Therefore, the CT specimens results are not the lowest, and thus are not conservative.

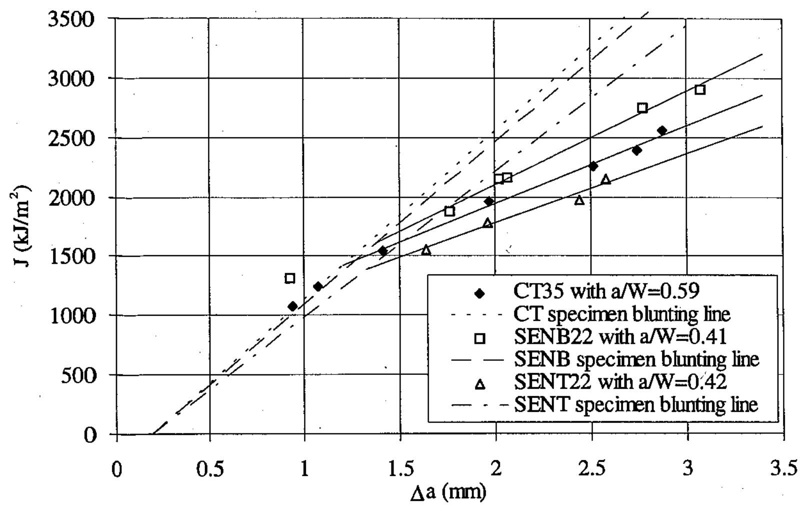

Figure 3 : Geometry effects on J-R curves for cracked specimens with 20% side-grooves.

3.2.5. Fracture toughness locus in 304L stainless steel at 300°C.

The global approach is applied on 304L stainless steel. The Q values are larger than those O'Downd and Shih[1] found. These values range from -9 to 0. It is interesting to notice that for higher deformation levels, the most negative values of Q are for bending specimens and not for tension ones. O'Downd and Shih[1] have observed another classification for lower deformations. J_a-Q or J_{Ic}-Q curve is monotonous and seems to be a representative toughness locus.

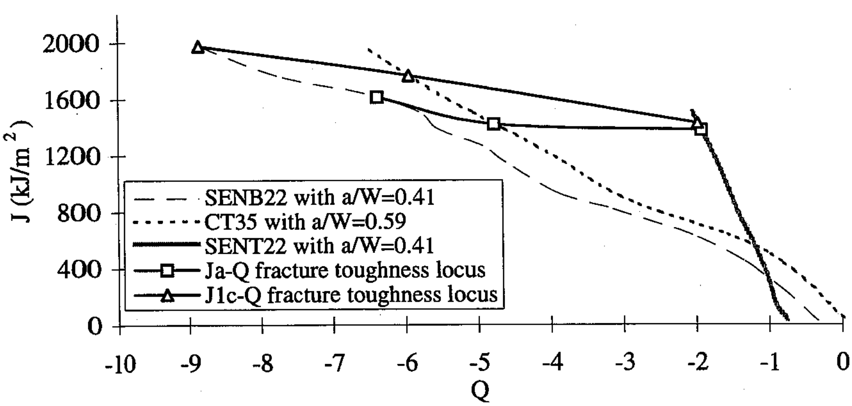

Figure 4 : Fracture toughness locus in 304L stainless steel at 300°C.

4. LOCAL APPROACH.

The local approach applies micromechanics models to predict the crack initiation and ductile tearing. We use two different models : the first one is based on critical cavity growth and the second couples a damage and yielding.

4.1. *Models based on critical cavity growth.*

The growth of an isolated void in an infinite block of an elastic perfectly plastic material is given by the Rice and Tracey[5] equation :

$$\ln\left(\frac{R}{R_0}\right)_c = \int_{\varepsilon_0}^{\varepsilon_R} 0.283 \exp\left(\frac{3}{2}\left|\frac{\sigma_m}{\sigma_{eq}}\right|\right) d\varepsilon_{eq}^{pl} \tag{16}$$

where R is the actual cavity size, R_0 the initial cavity size, ε_R defined in the previous section, is the strain at failure, ε_0 is the initial strain at nucleation and assumed to be equal to zero. Budiansky[6]'s model for an isolated axisymmetric void is developed for a non linear elastic plastic material. The dilatation rate of a void is :

$$\ln\left(\frac{V}{V_0}\right)_c = \int_{\varepsilon_0}^{\varepsilon_R} \alpha \frac{3}{2}\left\{\frac{3n}{2}\left|\frac{\sigma_m}{\sigma_{eq}}\right| + (1+n)\cdot(1+0.418n+\alpha 0.0144n)\right\}^{1/n} d\varepsilon_{eq}^{pl} \tag{17}$$

where $\alpha = \mathrm{sign}(\sigma_m)$, V is the actual cavity volume and V_0 the initial cavity volume. The work-hardening exponent n is given in Table 1.

4.2. *Models based on damage theory.*

Tai and Yang[7] proposed the following damage criterion for ductile tearing :

$$V_{Dc} = \int_{\varepsilon_0}^{\varepsilon_R} f(\sigma_m/\sigma_{eq})\, d\varepsilon_{eq}^{pl} \tag{18}$$

where $f(\sigma_m/\sigma_{eq}) = 2(1+\nu)/3 + 3(1-2\nu)\cdot(\sigma_m/\sigma_{eq})^2$. (19)

If the work-hardening exponent n is large, another damage failure criterion is assumed to better take into account both work-hardening and plastic strain effects :

$$V_{DM} = \int_{\varepsilon_0}^{\varepsilon_R} f(\sigma_m/\sigma_{eq})\left(\varepsilon_{eq}^{pl}\right)^{2n} d\varepsilon_{eq}^{pl} \tag{20}$$

This second damage parameter V_{DM} is called modified Tai and Yang[7] damage parameter.

In order to apply the models, we need to identify two independent parameters : the critical value of the damage parameter (for which the failure is assumed to occur), and the critical size.

4.3. *Critical values of damage parameters.*

The determination of critical values $(R/R_0)_c$, $(V/V_0)_c$, $(V_D)_c$ and $(V_{DM})_c$ is performed on axisymmetric notched specimens AER. We present the results in **Figure 5** and **Figure 6** for the four models. The values of Rice&Tracey[5] and Tai&Yang[7] models are approximately constant and independent of stress triaxiality ratio. For the Tai&Yang[7] modified model (**Figure 6**), we notice that the V_{DM} values for AER10 specimens are slightly larger than for the other axisymmetric notched specimens. But for smaller stress triaxiality ratios, the V_{DM} values are roughly constant. Calculations from Budiansky and coll.[6] model give more scattered results (see **Figure 5**). Finally, it has been observed that an analysis based on AER specimens does not permit to distinguish the influence of work-hardening exponent n and plastic level on the models. The average values of $(R/R_0)_c$, $(V/V_0)_c$, $(V_D)_c$ and $(V_{DM})_c$ are presented in **Table 4** for the AER specimens.

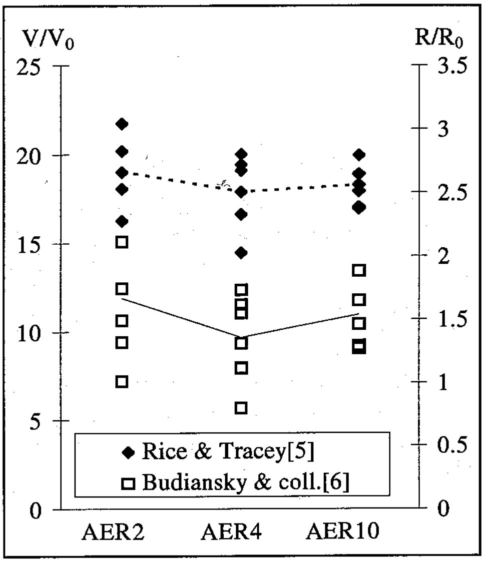

Figure 5 : Critical values of cavity growth criterion $(R/R_0)_c$ or $(V/V_0)_c$ for different notched specimens

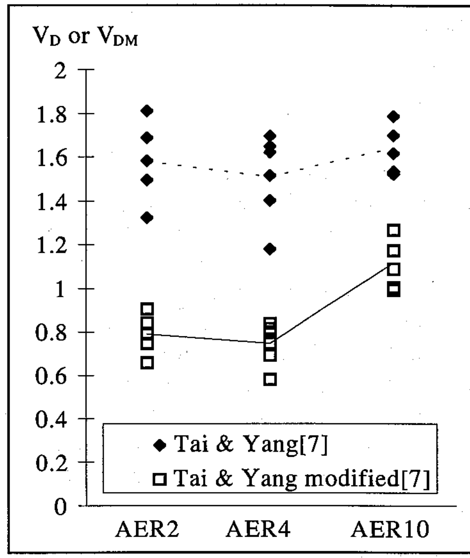

Figure 6 : Critical values of damage criterion $(V_D)_c$ or $(V_{DM})_c$ for different notched specimens

4.4. *Critical distances.*

This critical size λ_c is defined by the distance between the crack tip and the point where any of the previous criterion is reached. This parameter is fitted from calculations performed on SENT22 specimens with a/W=0.41. The critical distance λ_c values are tabulated on **Table 4.** Crack initiation (J_a or J_{Ic}) for CT35 specimens with a/W=0.59 and SENB22 specimens with a/W=0.41 is predicted to take place when the $(R/R_0)_c$, $(V/V_0)_c$, $(V_D)_c$ and $(V_{DM})_c$ values are reached at critical distance λ_c from the crack tip. The results for different models are presented in **Table 4.**

	J_a^{SENT}	J_a^{CT}	J_a^{SENB}		
Experiments	1328	1771	2041	**λ_c (mm)**	**$(R/R_0)_c$ - $(V/V_0)_c$ $(V_D)_c$ - $(V_{DM})_c$**
Rice & Tracey[5]	1380	680	700	1.6	2.6
Budiansky & coll.[6]	1380	1280	1250	1.9	10.76
Tai & Yang[7]	1380	1360	1320	1.8	1.6
Tai & Yang modified[7]	1380	1830	1695	1.15	0.82

Table 4 : Results from local approach models with critical size and critical values.

The results of Rice&Tracey[5], Budiansky and coll.[6] and Tai&Yang[7] models always lead to the same specimens classification, i. e., the lowest J_a values are for tension specimens and the larger J_a values are for bending specimens. It is interesting to notice that for Tai&Yang[7]

model, the J_a values were roughly constant (there are no effects of specimen geometries). The Budiansky and coll.[6] model takes the work-hardening exponent into account, but the classification of crack initiation is not modified. In **Table 4**, the Tai&Yang[7] modified values lead to another classification. The larger J_a values are correspond to CT specimens.
The classical approach which consists in averaging over characteristic volume or distance gives even worse results.

5. CONCLUSION.

Toughness experiments carried out on various specimen geometries showed as expected, the geometrical effect on J_{Ic} and J_a values. However, the lower values of J_{Ic} and J_a at crack initiation have been obtained on tension specimens. The (J-Q) technique gives one toughness fracture locus which provides a reasonable estimation of the geometry effects, but is not able to describe crack extension.
The prediction of specimen classification according to initiation toughness using the uncoupled models does not represented the measurement for 304L stainless steel. To this very ductile material, it seems necessary to take both work-hardening exponent and plastic strain into account for crack initiation. As a consequence, models coupling damage and plastic behaviour should be more suited to predict crack initiation and growth in these material. For that purpose, Gurson and Rousselier models are actually investigated.

REFERENCES :

1. O'Dowd, N. P & C. F. Shih 1992. Family of crack-tip fields characterised by a triaxiality parameter - II- Fracture applications.
Journal of the Mechanics and Physics of Solids 40 : 939-963.
2. Bauvineau, L. 1996. Approche locale de la rupture ductile : application à un acier Carbone-Manganèse.
Thesis.
3. Dawes, M. G., R. H. Leggatt & G. Slater 1990. An international research project to develop shallow crack fracture mechanics tests - European contribution.
Sixth progress report, 5574/20/90, December, The welding institute.
4. McMeeking, R. M. 1977. Finite deformation analysis of crack-tip opening in elastic-plastic materials and implications for fracture.
Journal of the Mechanics and Physics of Solids 25 : 357-381.
5. Rice, J. R. and D. M. Tracey 1968. On the ductile enlargement of void in triaxial stress fields.
Journal of the Mechanics and Physics of Solids 17 : 201-217.
6. Budiansky,B., J. W. Hutchinson & S. Slutsky 1982. Void growth and collapse in viscous solids.
Mechanics of solids - The Rodney hill 60th anniversary volume. Edited by H. G. Hopkins and M. J. Sewell : 13-45.
7. Tai, W. H. & B. Yang 1987.
Engineering Fracture of Mechanics 27 : 371-378.